

Magnetic switch and electronic properties in chromium-intercalated two-dimensional GeP₃

Dominike P. de A. Deus¹, Igor S. S. de Oliveira², João B. Oliveira³, Wanderlã L. Scopel⁴, and R. H. Miwa⁵


¹*Instituto Federal de Educação, Ciência e Tecnologia de Goiás, Departamento de Áreas Acadêmicas, Campus Jataí, Ormindá Vieira de Freitas 775, 75804-714 Jataí, GO, Brazil*

²*Departamento de Física, Universidade Federal de Lavras, C.P. 3037, 37200-000 Lavras, MG, Brazil*

³*Instituto Federal do Triângulo Mineiro, 38270-000 Ituiutaba, MG, Brazil*

⁴*Departamento de Física, Universidade Federal do Espírito Santo, Vitória, ES 29075-910, Brazil*

⁵*Instituto de Física, Universidade Federal de Uberlândia, C.P. 593, 38400-902 Uberlândia, MG, Brazil*

 (Received 19 November 2020; revised 26 February 2021; accepted 28 April 2021; published 13 May 2021)

Intercalation of foreign atoms in two-dimensional (2D) hosts has been considered a quite promising route to engineer the electronic and magnetic properties in 2D platforms. In the present study, we performed a first-principles theoretical investigation of the energetic stability and the magnetic/electronic properties of 2D GeP₃ doped by Cr atoms. Our total energy results reveal the formation of thermodynamically stable Cr doped GeP₃ bilayer and quadrilayer, characterized by interstitial Cr atoms lying in the van der Waals gap between the stacked GeP₃ layers. The Cr-doped systems become magnetic, and the magnetic ordering can be tuned through the application of compressive mechanical strain. Moreover, the systems are metallic, characterized by the emergence of strain-induced spin-polarized channels at the Fermi level. These findings reveal that the atomic intercalation offers a set of degree of freedom not only to design but also to control the magnetic/electronic properties by mechanical strain in 2D systems.

DOI: [10.1103/PhysRevMaterials.5.054002](https://doi.org/10.1103/PhysRevMaterials.5.054002)

I. INTRODUCTION

In the first decade of this century, material science has been marked by the emergence and development of two-dimensional (2D) materials. This interest started with the first isolation and characterization of graphene in 2004 [1]. Since then, many other 2D materials with graphenelike structures [2] have been theoretically predicted and/or synthesized [3], such as silicene, germanene, phosphorene, stanene [4–7], layered transition metal dichalcogenides [8], and transition metal carbides [9]. In these systems, the combination of quantum confinement and surface effects lead to novel physical properties, which can find a wide range of technological applications in the development of electronic devices based on 2D platforms [10,11].

Among the newly discovered 2D materials over recent years, the structural stability and the emergence of interesting electronic and magnetic properties in various 2D metal triphosphides have been reported, namely BP₃ [12], SnP₃ [13,14], CaP₃ [15], GeP₃ [16–18], and InP₃ [19]. In general, they all present moderate band gaps, adjustable through strain and stacking engineering, high carrier mobility, and strong light absorption in the visible and ultraviolet regions. Similarly to SnP₃, the layered structure of germanium triphosphide (GeP₃) has long been synthesized [16,17]. It consists of chemically bonded (Ge/P) atoms where the P atoms form buckled hexagonal structures connected by Ge atoms, resulting in GeP₃ sheets which in turn are stacked mediated by van der Waals (vdW) interactions. Recently, Jing *et al.* [18] have shown that few layers GeP₃ are chemically, mechanically, and dynamically stable by means of first principles calculations.

The monolayer and bilayer GeP₃ are also characterized by high carrier mobility and solar light absorption, desirable properties in photovoltaic cells, while the trilayer system is metallic. These properties, combined with the prediction of experimentally accessible cleavage energies, have promoted a number of studies focusing on possible applications [20,21] and new features hosted in GeP₃. For instance, the control of electronic mobility and band structure through strain engineering [22], substitutional doping in the GeP₃ monolayer [23], and the electronic transport properties in nanoribbons [24,25].

Further investigations on 2D metal triphosphides revealed that InP₃ monolayer presents tuneable magnetism upon hole doping, resulting in a ferromagnetic state ruled by P(3*p*) orbitals [19]. Indeed, magnetism in two-dimensional systems, and its control mediated by external agents, have been the subject of intense research works, addressing fundamental [26] and technological aspects. For instance, currently, there is an intense quest for new 2D magnetic materials, aiming for application in spintronic engineering. Since the recent experimental verification of intrinsic magnetic order in (layered) vdW crystals of Cr₂Ge₂Te₆ [27] and CrI₃ [28], other 2D magnetic crystals have been predicted in the recent literature [29–34]. In addition to the material synthesis, the suitable control of the magnetic properties in 2D platforms has been an important challenge in order to design new spintronic devices. In fact, there are several proposals addressing such control, for instance, carrier doping [35–37], mechanical strain [38–40], external electric field [41–43], pressure [44–48], and (more recently) through atomic intercalation [49–56]. In parallel to the experimental realizations, ongoing theoretical studies

based on first-principles simulations have delivered important contributions to the atomistic understanding of the electronic and magnetic properties of 2D systems.

In this work we show the possibility of inducing magnetic properties in germanium triphosphide upon the intercalation of foreign atoms (Cr) and further control of the magnetic and electronic properties by an external agent (mechanical pressure). Based on first-principles calculations, we investigate the energetic stability, magnetic, and electronic properties of the GeP_3 bilayer $[(\text{GeP}_3)_{\text{BL}}]$ intercalated with interstitial Cr atoms $[(\text{GeP}_3)_{\text{BL}}^{\text{Cr}}]$, and its stacked counterparts, namely $(\text{GeP}_3)_{\text{BL}}^{\text{Cr}}/(\text{GeP}_3)_{\text{BL}}^{\text{Cr}}$, and the Cr intercalated $(\text{GeP}_3)_{\text{BL}}^{\text{Cr}}/\text{Cr}/(\text{GeP}_3)_{\text{BL}}^{\text{Cr}}$. We show that the investigated systems present tuneable magnetic phases induced by mechanical compressive strain, characterized by an intralayer AFM to FM transition in $(\text{GeP}_3)_{\text{BL}}^{\text{Cr}}$, and interlayer FM and AFM couplings in $(\text{GeP}_3)_{\text{BL}}^{\text{Cr}}/(\text{GeP}_3)_{\text{BL}}^{\text{Cr}}$ and $(\text{GeP}_3)_{\text{BL}}^{\text{Cr}}/\text{Cr}/(\text{GeP}_3)_{\text{BL}}^{\text{Cr}}$, respectively. Further electronic band structure calculations reveal the emergence of strain-induced spin-polarized channels at the Fermi level. These findings suggest that Cr-intercalated GeP_3 is an interesting building block to the design of 2D electronic devices, based on metal triphosphide materials, with tuneable electronic and magnetic functionalities.

II. RESULTS AND DISCUSSION

A. Cr-doped GeP_3 bilayer

Atomic intercalation in the vdW gaps of layered systems has been considered a promising strategy in order to control the electronic and magnetic properties of bulk materials [57,58] as well as their 2D counterparts [49–54], where, by taking advantage of the interface geometry, the intercalants may form periodic arrays between the stacked layers. Here, we examine the energetic stability, the magnetic/electronic properties of $(\text{GeP}_3)_{\text{BL}}$ doped by Cr atoms, and the control of these properties by applying an external (uniaxial) pressure.

Firstly, we have considered three plausible configurations for adsorbing the Cr atoms in the $(\text{GeP}_3)_{\text{BL}}$ structure (Fig. S1 in the Supplemental Material [59]). In Fig. 1(a) we present the lowest energy configuration, characterized by a layer of Cr atoms occupying the rhombohedral room between the GeP_3 MLs $[(\text{GeP}_3)_{\text{BL}}^{\text{Cr}}]$. The energetic stability of $(\text{GeP}_3)_{\text{BL}}^{\text{Cr}}$ was verified through the calculation of its formation energy [E^f , Eq. (1) in the Supplemental Material], where

we found $E^f = -20 \text{ meV}/\text{\AA}^2$. In addition, further structural stability was confirmed by performing *ab initio* molecular dynamics (AIMD) simulations at 300 K (Fig. S2 in the Supplemental Material).

In $(\text{GeP}_3)_{\text{BL}}^{\text{Cr}}$, the Cr atoms occupy all the rhombohedral rooms between the AB stacked layers of GeP_3 resulting in a triangular lattice of Cr atoms, corresponding to a coverage of half a monolayer (1/2 ML) compared with the one of Ge atoms, Fig. 1(b), giving rise to a δ -doping like structure. Interestingly, this formation resembles the experimentally observed boron δ -doping structure in $\text{B:Si}(111)-(\sqrt{3} \times \sqrt{3})\text{R}30^\circ$ for a B coverage of 1/3 of ML forming a periodic 2D structure [60–62]. Very recently, similar metal δ -doped structures have been verified in $\text{Fe}_{1/3}$, $\text{Co}_{1/3}$, and Cu intercalated transition metal dichalcogenides [57,63–66], and for coverages of 2/3 and one ML of Ta self-intercalated in $\text{TaS}(\text{Se})$ [53]. At the equilibrium geometry, the $(\text{GeP}_3)_{\text{BL}}^{\text{Cr}}$ lattice constants ($a = b = 7.05 \text{ \AA}$) and interlayer distance ($d = 2.11 \text{ \AA}$) are nearly the same as compared to the pristine $(\text{GeP}_3)_{\text{BL}}$ ($a = b = 7.08 \text{ \AA}$ and $d = 2.09 \text{ \AA}$, see Fig. S3 in the Supplemental Material), thus indicating that the local atomic structure of $(\text{GeP}_3)_{\text{BL}}$ is weakly perturbed by the presence of the interstitial Cr atoms. We found Cr-P and Cr-Ge bond lengths of 2.59 and 3.17 \AA , respectively, which are slightly larger than the sum of their covalent radii, resulting in an increase of the vertical distance h from 5.05 to 6.34 \AA [Fig. S3(a) in the Supplemental Material and Fig. 1(a)].

The interstitial Cr atoms present a net magnetic moment of 3.4 μ_{B} , which are coupled mediated by the P atoms. We have compared the energetic stability of four magnetic phases [67], as shown in Figs. 2(a1)–2(a4). At the equilibrium geometry, we found the row-wise antiferromagnetic (RW-AFM) phase [Fig. 2(a1), hereafter labeled as $\text{Cr}^{\uparrow\downarrow}$] as the most stable spin configuration, and the ferromagnetic (FM) phase [Fig. 2(a4), hereafter labeled as $\text{Cr}^{\uparrow\uparrow}$] as the least stable one by $E_{\text{RW-AFM}} - E_{\text{FM}} = -59 \text{ meV}/\text{Cr}$. Interestingly, the energetic preference for the AFM coupling between two nearest neighbor Cr atoms has been preserved even at lower concentration regime. That is, for a coverage of 1/9 ML, we found the AFM configuration more stable than the FM one by 117 meV/Cr (details in Fig. S4 of the Supplemental Material).

We found that the energetic preference for the RW-AFM alignment in $(\text{GeP}_3)_{\text{BL}}^{\text{Cr}}$ can be tuned by mechanical compressive strain, $\varepsilon = (h_0 - h)/h_0$, where h_0 (h) are the vertical distances between the topmost and bottommost atomic layer of the unstrained (strained) $(\text{GeP}_3)_{\text{BL}}^{\text{Cr}}$. The values of the applied pressure (P) as a function of the interlayer distance are computed according to

$$P(h) = \frac{\Delta E}{A_{xy}|\Delta h|},$$

where $\Delta E = E_{i+1} - E_i$ is the total energy difference between the $(i+1)$ th and i th configurations, and Δh is the respective reduction of the vertical distance ($\Delta h = h_{i+1} - h_i$) between the topmost and bottommost atomic layer of $(\text{GeP}_3)_{\text{BL}}^{\text{Cr}}$. A_{xy} is the unit cell surface area of the $(i+1)$ th configuration. Here $i = 0$ corresponds to the unstrained geometry. In Fig. 2(b) we present our results of $E_{\text{RW-AFM}} - E_{\text{FM}}$ as a function of the pressure. A $\text{Cr}^{\uparrow\downarrow} \xrightarrow{\varepsilon} \text{Cr}^{\uparrow\uparrow}$ magnetic transition for P is

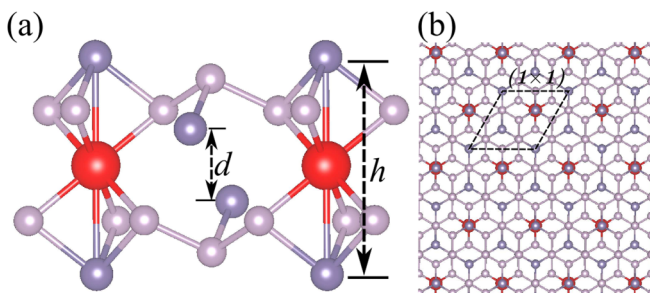


FIG. 1. Structural model of Cr doped $(\text{GeP}_3)_{\text{BL}}$, side (a) and top (b) views. The separation distance between top and bottom Ge atoms on $(\text{GeP}_3)_{\text{BL}}^{\text{Cr}}$, and the spacing between the individual layers in GeP_3 are indicated by h and d , respectively.

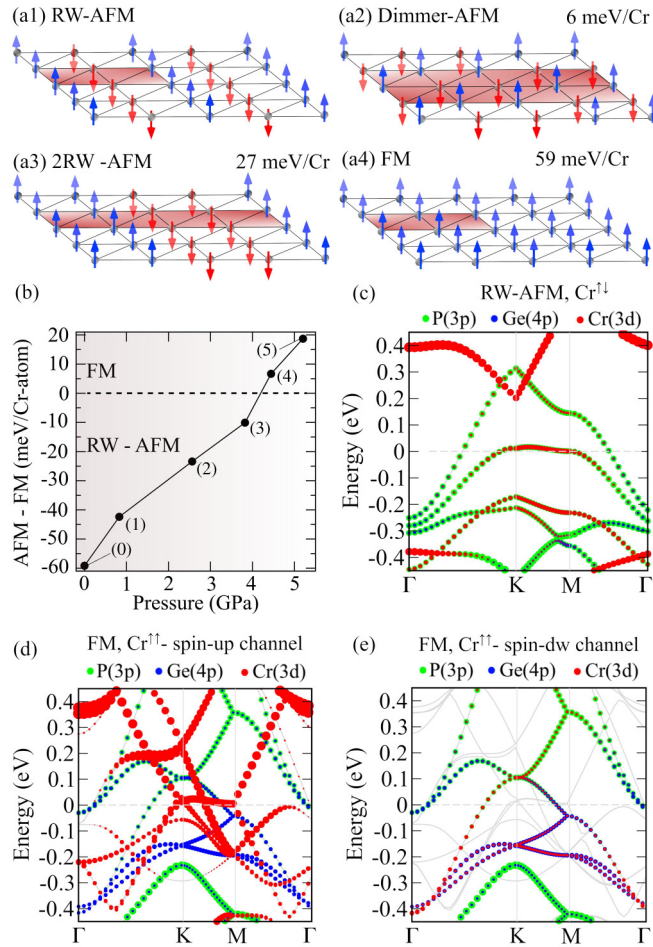


FIG. 2. Magnetic configurations models of $(\text{GeP}_3)_{\text{BL}}^{\text{Cr}}$, (a1) row-wise antiferromagnetic (RW-AFM), (a2) Dimmer-AFM, (a3) 2RW-AFM, and (a4) ferromagnetic (FM) phases. (b) Total energy difference between RW-AFM and FM phases as a function of the external compressive strain. The configuration index (i) is indicated between parenthesis. Orbital projected electronic band structures of the uncompressed ($h = 6.34 \text{ \AA}$) RW-AFM $(\text{GeP}_3)_{\text{BL}}^{\text{Cr}}$ (c), and compressed ($h = 5.07 \text{ \AA}$) FM $(\text{GeP}_3)_{\text{BL}}^{\text{Cr}}$, spin-up (d) and -down (e) channels.

noticeable between 3.8 and 4.4 GPa. Upon further compression the FM phase becomes more stable by $E_{\text{RW-AFM}} - E_{\text{FM}} = +21 \text{ meV/Cr}$, for $P = 5.2 \text{ GPa}$ ($\epsilon \approx 20\%$). It is worth pointing out that the maximum pressure applied here is comparable with those applied in other 2D vdW structures [44,47,68], thus supporting the feasibility of such a magnetic tuning. Further total energy comparisons between the FM phase and the other magnetic configurations (Dimmer-AFM and 2RW-AFM) confirm its energetic preference by +31 and +22 meV/Cr, respectively, for $P = 5.2 \text{ GPa}$. These values of total energy difference between the FM and AFM phases ($\Delta E_{\text{AFM-FM}}$), combined with the mean-field theory [69–71], allow us to provide an estimation of the Curie temperature (T_C) using $k_B T_C = (2/3)\Delta E_{\text{AFM-FM}}$. We found that, at $P = 5.2 \text{ GPa}$, the intralayer FM phase ($\text{Cr}^{\uparrow\uparrow}$) presents T_C of about 162 K.

The orbital projected electronic band structure of the RW-AFM $(\text{GeP}_3)_{\text{BL}}^{\text{Cr}}$, Fig. 2(c), reveals the formation of metallic bands mostly ruled by the P($3p$), while the Cr atoms give rise

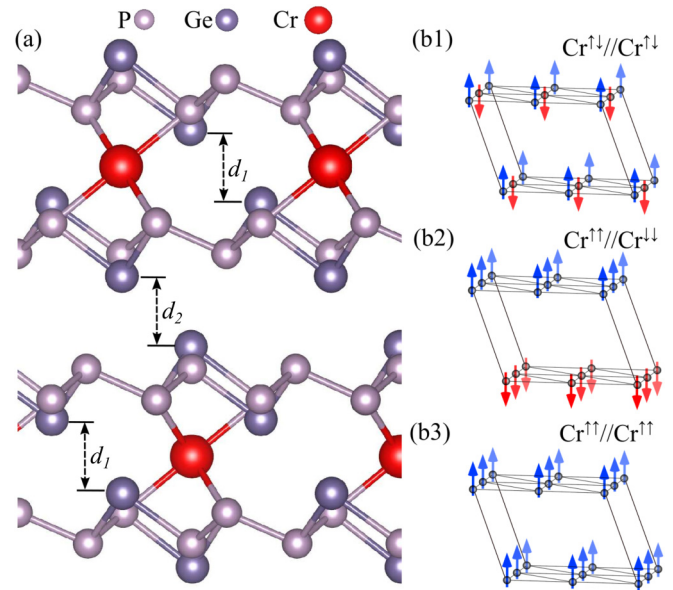


FIG. 3. (a) Structural model of $(\text{GeP}_3)_{\text{BL}}^{\text{Cr}}/(\text{GeP}_3)_{\text{BL}}^{\text{Cr}}$, and the schematic spin configurations $\text{Cr}^{\uparrow\downarrow}/\text{Cr}^{\uparrow\downarrow}$ (b1), $\text{Cr}^{\uparrow\uparrow}/\text{Cr}^{\uparrow\downarrow}$ (b2), and $\text{Cr}^{\uparrow\uparrow}/\text{Cr}^{\uparrow\uparrow}$ (b3). The localization and the spin polarization of the Cr atom are indicated by arrows. The interface distances are indicated by d_1 and d_2 in (a).

to localized states resonant with the Fermi level along the KM direction. In contrast, the spin-up and -down energy bands are no longer degenerated upon compression, Figs. 2(d) and 2(e). The spin-up channel presents a larger density of states near the Fermi level compared with that of the spin-down channel. The former can be characterized by Cr($3d$) bands along the KM direction, one dispersionless and the other with nearly linear dispersion crossing the Fermi level. The presence of both spin channels at the Fermi level, and the predominance of spin-up metallic bands, with respect to those of spin-down, indicates the emergence of mechanically tuneable partially spin-polarized electronic transport along the $(\text{GeP}_3)_{\text{BL}}^{\text{Cr}}$ layers.

B. $(\text{GeP}_3)_{\text{BL}}^{\text{Cr}}$ interfaces

The stacking of 2D magnetic systems is a quite interesting option for the search of new phenomena ruled by interlayer interactions. For instance, magnetic phases in a few layers CrI_3 as a function of the stacking geometry [42] that in turn can be tuned by external agents like electric field [43] or mechanical pressure [44,45]. Here, we investigate the tuning of the magnetic properties of $(\text{GeP}_3)_{\text{BL}}^{\text{Cr}}$ bilayers mediated by vertical compressive strain. Firstly we have considered the stacking of two Cr doped $(\text{GeP}_3)_{\text{BL}}$, $(\text{GeP}_3)_{\text{BL}}^{\text{Cr}}/(\text{GeP}_3)_{\text{BL}}^{\text{Cr}}$, and then the intercalation of Cr atoms, $(\text{GeP}_3)_{\text{BL}}^{\text{Cr}}/\text{Cr}/(\text{GeP}_3)_{\text{BL}}^{\text{Cr}}$. It is worth noting that such a compression will promote two concurrent magnetic interactions, (i) the intralayer RW-AFM \rightarrow FM transition discussed above and (ii) proximity effects at $(\text{GeP}_3)_{\text{BL}}^{\text{Cr}}-(\text{GeP}_3)_{\text{BL}}^{\text{Cr}}$ interface.

In Fig. 3(a) we present the structural model of $(\text{GeP}_3)_{\text{BL}}^{\text{Cr}}/(\text{GeP}_3)_{\text{BL}}^{\text{Cr}}$, where the GeP_3 layers are stacked following the conventional ABC stacking order of its bulk phase [18]. At the equilibrium geometry, the structural properties of each $(\text{GeP}_3)_{\text{BL}}^{\text{Cr}}$ are mostly preserved, for instance the vertical

TABLE I. Total energy differences (in meV/Cr) with respect to the energetically more stable spin configuration of the free (ΔE_{Free}) and compressed ($\Delta E_{\text{Compress}}$) $(\text{GeP}_3)_{\text{BL}}^{\text{Cr}}//(\text{GeP}_3)_{\text{BL}}^{\text{Cr}}$ and $(\text{GeP}_3)_{\text{BL}}^{\text{Cr}}/\text{Cr}/(\text{GeP}_3)_{\text{BL}}^{\text{Cr}}$ systems.

Structure	ΔE_{Free}	$\Delta E_{\text{Compress}}$
$\text{Cr}^{\uparrow\downarrow}//\text{Cr}^{\uparrow\downarrow}$	0	4
$\text{Cr}^{\uparrow\uparrow}//\text{Cr}^{\uparrow\downarrow}$	51	39
$\text{Cr}^{\uparrow\uparrow}//\text{Cr}^{\uparrow\uparrow}$	67	0
$\text{Cr}^{\uparrow\downarrow}/\text{Cr}^{\uparrow\downarrow}/\text{Cr}^{\uparrow\downarrow}$	0	38
$\text{Cr}^{\uparrow\uparrow}/\text{Cr}^{\uparrow\downarrow}/\text{Cr}^{\uparrow\uparrow}$	60	0
$\text{Cr}^{\uparrow\uparrow}/\text{Cr}^{\uparrow\uparrow}/\text{Cr}^{\uparrow\uparrow}$	20	33

distances d_1 and h of 2.06 and 6.44 Å, respectively. The interlayer spacing between the two $(\text{GeP}_3)_{\text{BL}}^{\text{Cr}}$ layers, $d_2 = 2.07$ Å, is also practically the same as compared with the pristine $(\text{GeP}_3)_{\text{BL}}$. There are no chemical bonds connecting the $(\text{GeP}_3)_{\text{BL}}^{\text{Cr}}$ layers, indicating that the energetic stability of the stacked system is ruled by vdW interactions. The energetic stability of the bilayer system was verified by the calculation of the formation energy [for $X=(\text{GeP}_3)_{\text{BL}}^{\text{Cr}}//(\text{GeP}_3)_{\text{BL}}^{\text{Cr}}$ in Eq. (1) of the Supplemental Material], where we obtained $E^f = -25$ meV/Å².

Focusing on the magnetic properties, we have examined three plausible magnetic configurations, namely, (i) each $(\text{GeP}_3)_{\text{BL}}^{\text{Cr}}$ layer presents RW-AFM alignment ($\text{Cr}^{\uparrow\downarrow}//\text{Cr}^{\uparrow\downarrow}$), (ii) the $(\text{GeP}_3)_{\text{BL}}^{\text{Cr}}$ layers present intralayer FM coupling and interlayer AFM coupling ($\text{Cr}^{\uparrow\uparrow}//\text{Cr}^{\uparrow\downarrow}$), and (iii) the $(\text{GeP}_3)_{\text{BL}}^{\text{Cr}}$ layers present intralayer and interlayer FM coupling ($\text{Cr}^{\uparrow\uparrow}//\text{Cr}^{\uparrow\uparrow}$). These spin configurations are schematically shown in Figs. 3(b1)–3(b3). Our total energy results reveal the former configuration, $\text{Cr}^{\uparrow\downarrow}//\text{Cr}^{\uparrow\downarrow}$, as the most stable one, followed by $\text{Cr}^{\uparrow\uparrow}//\text{Cr}^{\uparrow\downarrow}$ (+51 meV/Cr) and $\text{Cr}^{\uparrow\uparrow}//\text{Cr}^{\uparrow\uparrow}$ (+67 meV/Cr), respectively. The energy difference of 16 meV between these two intralayer FM phases indicates the

presence of magnetic coupling between the FM $(\text{GeP}_3)_{\text{BL}}^{\text{Cr}}$ layers, favoring the former one.

Such a magnetic coupling can be strengthened by a compressive strain normal to the stacking direction. In this case, concomitantly with the reduction of the vertical interlayer distance d_2 , the reduction of d_1 will favor the intralayer FM interaction between the Cr atoms, $\text{Cr}^{\uparrow\downarrow} \xrightarrow{\varepsilon} \text{Cr}^{\uparrow\uparrow}$. Indeed, for a compressive strain of $\varepsilon = 26\%$ ($P = 8.4$ GPa) there is an energetic preference for the intralayer and interlayer FM configuration [Fig. 3(b3)], thus characterizing a $\text{Cr}^{\uparrow\downarrow}/\text{Cr}^{\uparrow\downarrow} \xrightarrow{\varepsilon} \text{Cr}^{\uparrow\uparrow}/\text{Cr}^{\uparrow\uparrow}$ magnetic transition tuned by mechanical strain. Our total energy results are summarized in Table I. These results, in addition with the spin polarization of the Ge and P atoms at the interface region, suggest an indirect magnetic interaction between the $(\text{GeP}_3)_{\text{BL}}^{\text{Cr}}$ layers.

We have a quite different picture for the interlayer interaction upon the intercalation of Cr atoms, namely $(\text{GeP}_3)_{\text{BL}}^{\text{Cr}}/\text{Cr}/(\text{GeP}_3)_{\text{BL}}^{\text{Cr}}$. The Cr atoms lie in the rhombohedral room between the $(\text{GeP}_3)_{\text{BL}}^{\text{Cr}}$ layers [Fig. 4(a)], giving rise to Cr δ -doped GeP_3 quadrilayers $[(\text{GeP}_3)_{\text{QL}}^{\text{Cr}}]$. The energetic stability of $(\text{GeP}_3)_{\text{QL}}^{\text{Cr}}$ was confirmed by the calculation of its formation energy, where we found E^f of -21 meV/Å². At the optimized geometry, $(\text{GeP}_3)_{\text{QL}}^{\text{Cr}}$ presents interlayer distances of $d_1 = 2.00$ Å, and $d_2 = 2.04$ Å, while the undoped pristine GeP_3 quadrilayer presents equally spaced interlayer distances of 1.97 Å.

Next we investigate the magnetic coupling between the Cr atoms. We have considered the spin configurations presented in Figs. 4(b1)–4(b3), hereafter labeled as $\text{Cr}^{\uparrow\downarrow}/\text{Cr}^{\uparrow\downarrow}/\text{Cr}^{\uparrow\downarrow}$, $\text{Cr}^{\uparrow\uparrow}/\text{Cr}^{\uparrow\downarrow}/\text{Cr}^{\uparrow\uparrow}$, and $\text{Cr}^{\uparrow\uparrow}/\text{Cr}^{\uparrow\uparrow}/\text{Cr}^{\uparrow\uparrow}$. At the equilibrium geometry, we found the former spin configuration [where each $(\text{GeP}_3)_{\text{BL}}^{\text{Cr}}$ is characterized by the RW-AFM alignment] more stable than the other ones by 20 and 60 meV/Cr, respectively. However, for a pressure of about 6.2 GPa ($\varepsilon = 22\%$), $\text{Cr}^{\uparrow\uparrow}/\text{Cr}^{\uparrow\downarrow}/\text{Cr}^{\uparrow\uparrow}$ [Fig. 4(b2)]

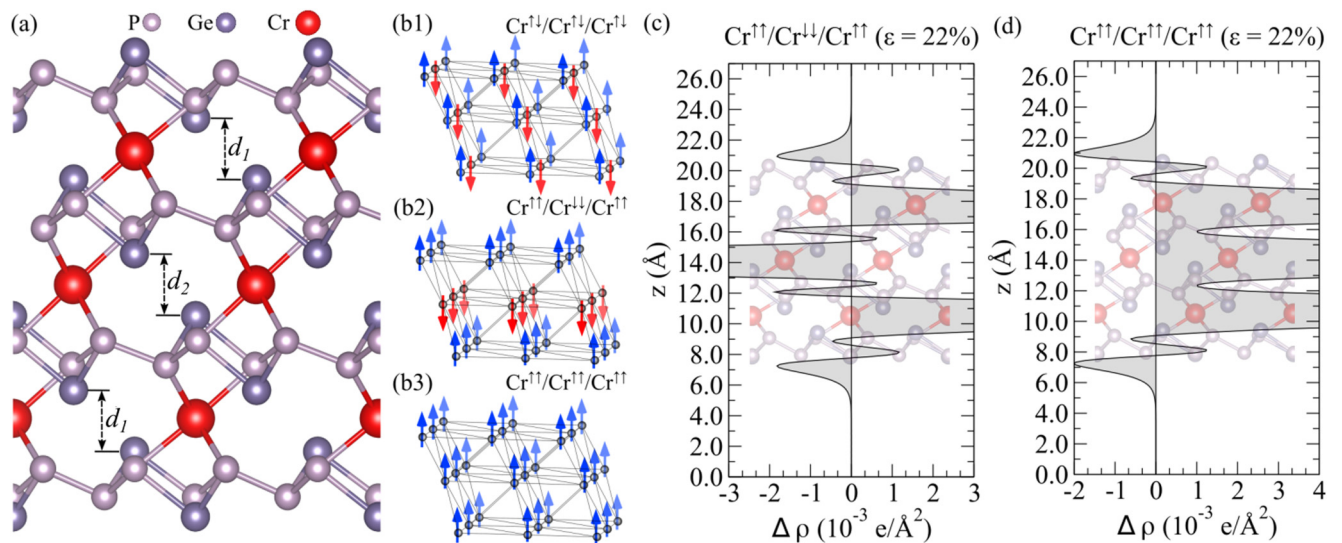


FIG. 4. (a) Structural model of $(\text{GeP}_3)_{\text{BL}}^{\text{Cr}}/\text{Cr}/(\text{GeP}_3)_{\text{BL}}^{\text{Cr}}$, and the spin configurations $\text{Cr}^{\uparrow\downarrow}/\text{Cr}^{\uparrow\downarrow}/\text{Cr}^{\uparrow\downarrow}$ (b1), $\text{Cr}^{\uparrow\uparrow}/\text{Cr}^{\uparrow\downarrow}/\text{Cr}^{\uparrow\uparrow}$ (b2), and $\text{Cr}^{\uparrow\uparrow}/\text{Cr}^{\uparrow\uparrow}/\text{Cr}^{\uparrow\uparrow}$ (b3). The localization and the spin polarization of the Cr atom are indicated by arrows. Planar averaged spin density along the z axis of the compressed $(\text{GeP}_3)_{\text{BL}}^{\text{Cr}}/\text{Cr}/(\text{GeP}_3)_{\text{BL}}^{\text{Cr}}$ system, $\text{Cr}^{\uparrow\uparrow}/\text{Cr}^{\uparrow\downarrow}/\text{Cr}^{\uparrow\uparrow}$ (c) and $\text{Cr}^{\uparrow\uparrow}/\text{Cr}^{\uparrow\uparrow}/\text{Cr}^{\uparrow\uparrow}$ (d). The interface distances are indicated by d_1 and d_2 in (a).

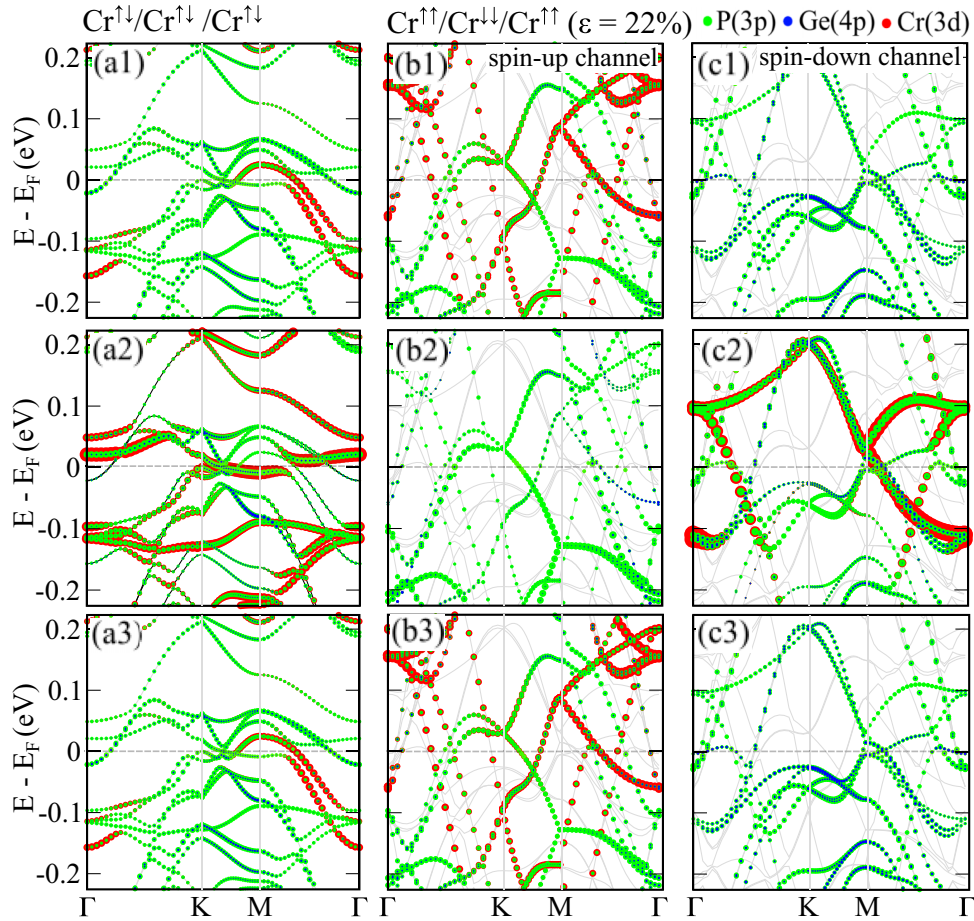


FIG. 5. The orbital projected electronic band structures of uncompressed (a) $\text{Cr}^{\uparrow\downarrow}/\text{Cr}^{\uparrow\downarrow}/\text{Cr}^{\uparrow\downarrow}$ and compressed [(b) spin-up, and (c) spin-down] $\text{Cr}^{\uparrow\uparrow}/\text{Cr}^{\downarrow\downarrow}/\text{Cr}^{\uparrow\uparrow}$ systems, projected on the top (a1)–(c1), central (a2)–(c2), and bottom (a3)–(c3) layers of $(\text{GeP}_3)_{\text{BL}}^{\text{Cr}}/\text{Cr}/(\text{GeP}_3)_{\text{BL}}^{\text{Cr}}$.

becomes more stable than $\text{Cr}^{\uparrow\uparrow}/\text{Cr}^{\uparrow\uparrow}/\text{Cr}^{\uparrow\uparrow}$ and $\text{Cr}^{\uparrow\downarrow}/\text{Cr}^{\uparrow\downarrow}/\text{Cr}^{\uparrow\downarrow}$ by 33 and 38 meV/Cr. Thus, revealing that $(\text{GeP}_3)_{\text{BL}}^{\text{Cr}}/\text{Cr}/(\text{GeP}_3)_{\text{BL}}^{\text{Cr}}$ also presents a tuneable spin configuration, namely $\text{Cr}^{\uparrow\downarrow}/\text{Cr}^{\uparrow\downarrow}/\text{Cr}^{\uparrow\downarrow} \xrightarrow{\varepsilon} \text{Cr}^{\uparrow\uparrow}/\text{Cr}^{\downarrow\downarrow}/\text{Cr}^{\uparrow\uparrow}$. Based on the total energy differences presented in Table I, we can infer the Curie temperature for the intralayer FM magnetic couplings in the stacked systems and then compare with the compressed $(\text{GeP}_3)_{\text{BL}}^{\text{Cr}}$, where $T_C = 162$ K. Here, using the mean-field theory with $\Delta E_{\text{AFM-FM}} \equiv \Delta E_{\text{Compress}}$, we found that T_C reduces to 31 K in $(\text{GeP}_3)_{\text{BL}}^{\text{Cr}}/(\text{GeP}_3)_{\text{BL}}^{\text{Cr}}$ ($\Delta E_{\text{Compress}} = 4$ meV), while it increases to 294 K ($\Delta E_{\text{Compress}} = 38$ meV) upon the intercalation of Cr atoms, $(\text{GeP}_3)_{\text{BL}}^{\text{Cr}}/\text{Cr}/(\text{GeP}_3)_{\text{BL}}^{\text{Cr}}$.

In order to provide a more complete picture of the interlayer coupling in $(\text{GeP}_3)_{\text{QL}}^{\text{Cr}}$, we have examined the planar averaged spin density along the stacking direction (z) [$\Delta\rho^{\uparrow\downarrow}(z)$ defined in Eq. (2) of the Supplemental Material]. Our results of $\Delta\rho^{\uparrow\downarrow}(z)$ for the spin configurations $\text{Cr}^{\uparrow\uparrow}/\text{Cr}^{\downarrow\downarrow}/\text{Cr}^{\uparrow\uparrow}$ and $\text{Cr}^{\uparrow\uparrow}/\text{Cr}^{\uparrow\uparrow}/\text{Cr}^{\uparrow\uparrow}$ at $\varepsilon = 22\%$ are shown in Figs. 4(c) and 4(d). The net magnetic moments are mostly localized in the layers containing Cr atoms. However, in the $\text{Cr}^{\uparrow\uparrow}/\text{Cr}^{\downarrow\downarrow}/\text{Cr}^{\uparrow\uparrow}$ configuration the interface P atoms also become spin polarized. The energetic advantage of $\text{Cr}^{\uparrow\uparrow}/\text{Cr}^{\downarrow\downarrow}/\text{Cr}^{\uparrow\uparrow}$, in the compressed system, comes from a combination of (i) the $\text{Cr}^{\uparrow\downarrow} \xrightarrow{\varepsilon} \text{Cr}^{\uparrow\uparrow}$ transition within the $(\text{GeP}_3)_{\text{BL}}^{\text{Cr}}$ units, and (ii) the lowering of the kinetic energy

ruled by a superexchange interaction, mediated by the interface P atoms [Fig. 4(c)]. As shown in Fig. 4(d), such (kinetic) energy gain is not allowed in $\text{Cr}^{\uparrow\uparrow}/\text{Cr}^{\uparrow\uparrow}/\text{Cr}^{\uparrow\uparrow}$.

Finally, focusing on the electronic properties, in Fig. 5(a) we present the orbital projected electronic band structure of the uncompressed $(\text{GeP}_3)_{\text{QL}}^{\text{Cr}}$. The projections on the edge $(\text{GeP}_3)_{\text{BL}}^{\text{Cr}}$ layers present the same band structures [Figs. 5(a1) and 5(a3)], where we find the formation of metallic bands, mostly composed by Cr(3d) and P(3p) hybridized states. Meanwhile, the electronic bands projected in the central layer are characterized by the presence of dispersionless Cr(3d) bands near the Fermi level, Fig. 5(a2). In the lowest energy configuration for $\varepsilon = 0$, $\text{Cr}^{\uparrow\downarrow}/\text{Cr}^{\uparrow\downarrow}/\text{Cr}^{\uparrow\downarrow}$, the spin-up and -down channels are degenerated. Such a degeneracy has been removed for $\varepsilon = 22\%$, where the $\text{Cr}^{\uparrow\uparrow}/\text{Cr}^{\downarrow\downarrow}/\text{Cr}^{\uparrow\uparrow}$ configuration becomes more stable. As shown in Figs. 5(b1) and 5(b3), for the spin-up channels the hybridization of Cr(3d) and P(3p) orbitals gives rise to metallic bands along the edge $(\text{GeP}_3)_{\text{BL}}^{\text{Cr}}$ layers. Meanwhile, the density of metallic states has been reduced in the central layer, with no projection of the Cr(3d) orbitals, Fig. 5(b2). The spin-down energy bands present a somewhat opposite picture, namely the Cr(3d) and P(3p) hybridized bands localized in the central $(\text{GeP}_3)_{\text{BL}}^{\text{Cr}}$ layer [Fig. 5(c2)], and absence of Cr(3d) orbital projection on the spin-down channels at the edge layers [Figs. 5(c1) and 5(c3)].

These findings reveal that, in addition to the spin configurations, the rise and (layer) localization of the spin-polarized metallic bands can also be tuned by mechanical strain in Cr intercalated GeP_3 systems.

III. CONCLUSIONS

We have performed an *ab initio* investigation of few layers GeP_3 doped by Cr atoms. The energetic and structural stabilities of Cr atoms lying in the rhombohedral room between GeP_3 layers, $(\text{GeP}_3)_{\text{BL}}^{\text{Cr}}$, have been verified through formation energy calculations and first-principles molecular dynamic simulations. We found that the ground state row-wise antiferromagnetic (RW-AFM) configuration in $(\text{GeP}_3)_{\text{BL}}^{\text{Cr}}$, $\text{Cr}^{\uparrow\downarrow}$, can be tuned to a ferromagnetic phase mediated by compressive mechanical strain (ε), $\text{Cr}^{\uparrow\downarrow} \xrightarrow{\varepsilon} \text{Cr}^{\uparrow\uparrow}$. Meanwhile, in the stacked systems, $(\text{GeP}_3)_{\text{BL}}^{\text{Cr}}/(\text{GeP}_3)_{\text{BL}}^{\text{Cr}}$, and $(\text{GeP}_3)_{\text{BL}}^{\text{Cr}}/\text{Cr}/(\text{GeP}_3)_{\text{BL}}^{\text{Cr}}$, we found that the ground state RW-AFM phase can be switched to layer by layer FM ($\text{Cr}^{\uparrow\uparrow}/\text{Cr}^{\uparrow\uparrow}$) and AFM ($\text{Cr}^{\uparrow\uparrow}/\text{Cr}^{\uparrow\downarrow}/\text{Cr}^{\uparrow\uparrow}$) phases, respectively. Concomitantly with such a magnetic tuning, further electronic structure calculations revealed the formation of metallic bands with the predominance of one spin channel with respect to the other. The predicted mechanical control of the electronic and magnetic properties, combined with the energetic and structural stabilities, suggest that $(\text{GeP}_3)_{\text{BL}}^{\text{Cr}}$ might be an interesting building block for the development of electronic/magnetic devices based on 2D platforms.

IV. COMPUTATIONAL APPROACH

The calculations were performed by using the density functional theory (DFT) as implemented in the QUANTUM ESPRESSO code [72]. The exchange correlation energy was described within the spin-polarized generalized gradient approximation, as proposed by Perdew, Burke, and Ernzerhof (GGA-PBE) [73], and further van der Waals (vdW) interactions were included using the vdW-DF approach [74–77]. Onsite Coulomb interaction (DFT+ U) has been included for Cr d orbitals [78]. The electron-ion interactions were described using the projector augmented wave potential (PAW) [79]. In addition, (i) we have confirmed some key results and (ii) performed *ab initio* molecular dynamic (AIMD) calculations by using the Vienna *ab initio* simulation package (VASP) [80]. Further calculation details are presented in the Supplemental Material.

ACKNOWLEDGMENTS

The authors acknowledge financial support from the Brazilian agencies CNPq, CAPES, FAPES and FAPEMIG; and the CENAPAD-SP (Centro Nacional de Processamento de Alto Desempenho-São Paulo), LNCC (Laboratório Nacional de Computação Científica, Projeto SCAFMAT2), and CENAPAD-UFC (Centro Nacional de Processamento de Alto Desempenho da Universidade Federal do Ceará) for computer time.

-
- [1] K. S. Novoselov, A. K. Geim, S. V. Morozov, D. Jiang, Y. Zhang, S. V. Dubonos, I. V. Grigorieva, and A. A. Firsov, *Science* **306**, 666 (2004).
- [2] S. Balendhran, S. Walia, H. Nili, S. Sriram, and M. Bhaskaran, *Small* **11**, 640 (2015).
- [3] R. Mas-Balleste, C. Gomez-Navarro, J. Gomez-Herrero, and F. Zamora, *Nanoscale* **3**, 20 (2011).
- [4] B. Lalmi, H. Oughaddou, H. Enriquez, A. Kara, S. V. B. Ealet, and B. Aufray, *Appl. Phys. Lett.* **97**, 223109 (2010).
- [5] M. Derivaz, D. Dentel, R. Stephan, M.-C. Hanf, A. Mehdaoui, P. Sonnet, and C. Pirri, *Nano Lett.* **15**, 2510 (2015).
- [6] L. Li, Y. Yu, G. J. Ye, Q. Ge, X. Ou, H. Wu, D. Feng, X. H. Chen, and Y. Zhang, *Nat. Nanotechnol.* **9**, 372 (2014).
- [7] F.-f. Zhu, W.-j. Chen, Y. Xu, C.-l. Gao, D.-d. Guan, C.-h. Liu, D. Qian, S.-C. Zhang, and J.-f. Jia, *Nat. Mater.* **14**, 1020 (2015).
- [8] M. Xu, T. Liang, M. Shi, and H. Chen, *Chem. Rev.* **113**, 3766 (2013).
- [9] I. Persson, J. Halim, H. Lind, T. W. Hansen, J. B. Wagner, L. A. k. Näslund, V. Darakchieva, J. Palisaitis, J. Rosen, and P. O. A. Persson, *Adv. Mater.* **31**, 1805472 (2019).
- [10] K. Novoselov, A. Mishchenko, A. Carvalho, and A. C. Neto, *Science* **353**, aac9439 (2016).
- [11] K. Khan, A. K. Tareen, M. Aslam, R. Wang, Y. Zhang, A. Mahmood, Z. Ouyang, H. Zhang, and Z. Guo, *J. Mater. Chem. C* **8**, 387 (2020).
- [12] F. Shojaei and H. S. Kang, *J. Mater. Chem. C* **5**, 11267 (2017).
- [13] S. Sun, F. Meng, H. Wang, H. Wang, and Y. Ni, *J. Mater. Chem. A* **6**, 11890 (2018).
- [14] B. Ghosh, S. Puri, A. Agarwal, and S. Bhowmick, *J. Phys. Chem. C* **122**, 18185 (2018).
- [15] N. Lu, Z. Zhuo, H. Guo, P. Wu, W. Fa, X. Wu, and X. C. Zeng, *J. Phys. Chem. Lett.* **9**, 1728 (2018).
- [16] P. Donohue and H. Young, *J. Solid State Chem.* **1**, 143 (1970).
- [17] J. Gullman and O. Olofsson, *J. Solid State Chem.* **5**, 441 (1972).
- [18] Y. Jing, Y. Ma, Y. Li, and T. Heine, *Nano Lett.* **17**, 1833 (2017).
- [19] N. Miao, B. Xu, N. C. Bristowe, J. Zhou, and Z. Sun, *J. Am. Chem. Soc.* **139**, 11125 (2017).
- [20] F. Niu, M. Cai, J. Pang, X. Li, G. Zhang, and D. Yang, *Surf. Sci.* **684**, 37 (2019).
- [21] B. Tian, T. Huang, J. Guo, H. Shu, Y. Wang, and J. Dai, *Vacuum* **164**, 181 (2019).
- [22] B. Zeng, M. Long, X. Zhang, Y. Dong, M. Li, Y. Yi, and H. Duan, *J. Phys. D* **51**, 235302 (2018).
- [23] S. Zhang, R. Li, X. Fu, Y. Zhao, C. Niu, C. Li, Z. Zeng, S. Wang, C. Xia, and Y. Jia, *Nanoscale Res. Lett.* **14**, 307 (2019).
- [24] Q. Wang, J.-W. Li, B. Wang, and Y.-H. Nie, *Front. Phys.* **13**, 138501 (2018).
- [25] R. Li, X. Huang, X. Ma, Z. Zhu, C. Li, C. Xia, Z. Zeng, and Y. Jia, *Phys. Chem. Chem. Phys.* **21**, 275 (2019).
- [26] C. Vaz, J. Bland, and G. Lauhoff, *Rep. Prog. Phys.* **71**, 056501 (2008).
- [27] C. Gong, L. Li, Z. Li, H. Ji, A. Stern, Y. Xia, T. Cao, W. Bao, C. Wang, Y. Wang, Z. Q. Qiu, R. J. Cava, S. G. Louie, J. Xia, and X. Zhang, *Nature (London)* **546**, 265 (2017).
- [28] B. Huang, G. Clark, E. Navarro-Moratalla, D. R. Klein, R. Cheng, K. L. Seyler, D. Zhong, E. Schmidgall, M. A. McGuire, D. H. Cobden, W. Yao, D. Xiao, P. Jarillo-Herrero, and X. Xu, *Nature (London)* **546**, 270 (2017).

- [29] M.-W. Lin, H. L. Zhuang, J. Yan, T. Z. Ward, A. A. Puretzky, C. M. Rouleau, Z. Gai, L. Liang, V. Meunier, B. G. Sumpter *et al.*, *J. Mater. Chem. C* **4**, 315 (2016).
- [30] C. Gong and X. Zhang, *Science* **363**, eaav4450 (2019).
- [31] M. Gibertini, M. Koperski, A. F. Morpurgo, and K. S. Novoselov, *Nat. Nanotechnol.* **14**, 408 (2019).
- [32] S. Chabungbam and P. Sen, *Phys. Rev. B* **96**, 045404 (2017).
- [33] H. L. Zhuang, Y. Xie, P. R. C. Kent, and P. Ganesh, *Phys. Rev. B* **92**, 035407 (2015).
- [34] N. Miao, B. Xu, L. Zhu, J. Zhou, and Z. Sun, *J. Am. Chem. Soc.* **140**, 2417 (2018).
- [35] S. Jiang, L. Li, Z. Wang, K. F. Mak, and J. Shan, *Nat. Nanotechnol.* **13**, 549 (2018).
- [36] T. Cao, Z. Li, and S. G. Louie, *Phys. Rev. Lett.* **114**, 236602 (2015).
- [37] X. Li, X. Wu, and J. Yang, *J. Am. Chem. Soc.* **136**, 11065 (2014).
- [38] J. Jiao, N. Miao, Z. Li, Y. Gan, J. Zhou, and Z. Sun, *J. Phys. Chem. Lett.* **10**, 3922 (2019).
- [39] X. Chen, J. Qi, and D. Shi, *Phys. Lett. A* **379**, 60 (2015).
- [40] S. Chabungbam, S. Mohakud, and S. Dutta, *ACS Appl. Electron. Mater.* **2**, 3171 (2020).
- [41] S. Jiang, J. Shan, and K. F. Mak, *Nat. Mater.* **17**, 406 (2018).
- [42] P. Jiang, C. Wang, D. Chen, Z. Zhong, Z. Yuan, Z.-Y. Lu, and W. Ji, *Phys. Rev. B* **99**, 144401 (2019).
- [43] E. S. Morell, A. León, R. H. Miwa, and P. Vargas, *2D Materials* **6**, 025020 (2019).
- [44] T. Song, Z. Fei, M. Yankowitz, Z. Lin, Q. Jiang, K. Hwangbo, Q. Zhang, B. Sun, T. Taniguchi, K. Watanabe *et al.*, *Nat. Mater.* **18**, 1298 (2019).
- [45] T. Li, S. Jiang, N. Sivasdas, Z. Wang, Y. Xu, D. Weber, J. E. Goldberger, K. Watanabe, T. Taniguchi, C. J. Fennie *et al.*, *Nat. Mater.* **18**, 1303 (2019).
- [46] N. Miao, W. Li, L. Zhu, B. Xu, J. Zhou, S. R. Elliott, and Z. Sun, *Nanoscale Horiz.* **5**, 1566 (2020).
- [47] Y. Sun, R. Xiao, G. Lin, R. Zhang, L. Ling, Z. Ma, X. Luo, W. Lu, Y. Sun, and Z. Sheng, *Appl. Phys. Lett.* **112**, 072409 (2018).
- [48] S. Chen, V. L. Johnson, D. Donadio, and K. J. Koski, *J. Chem. Phys.* **153**, 124701 (2020).
- [49] H. Wang, H. Yuan, S. S. Hong, Y. Li, and Y. Cui, *Chem. Soc. Rev.* **44**, 2664 (2015).
- [50] J. Wan, S. D. Lacey, J. Dai, W. Bao, M. S. Fuhrer, and L. Hu, *Chem. Soc. Rev.* **45**, 6742 (2016).
- [51] R. H. Miwa, P. Venezuela, and E. S. Morell, *Phys. Rev. B* **92**, 115419 (2015).
- [52] Y. Gong, H. Yuan, C.-L. Wu, P. Tang, S.-Z. Yang, A. Yang, G. Li, B. Liu, J. van de Groep, M. L. Brongersma *et al.*, *Nat. Nanotechnol.* **13**, 294 (2018).
- [53] X. Zhao, P. Song, C. Wang, A. C. Riis-Jensen, W. Fu, Y. Deng, D. Wan, L. Kang, S. Ning, J. Dan *et al.*, *Nature (London)* **581**, 171 (2020).
- [54] Z. Wang, R. Li, C. Su, and K. P. Loh, *SmartMat* **1**, e1013 (2020).
- [55] Y. Tanaka, H. Matsuoka, M. Nakano, Y. Wang, S. Sasakura, K. Kobayashi, and Y. Iwasa, *Nano Lett.* **20**, 1725 (2020).
- [56] M. Rajapakse, B. Karki, U. O. Abu, S. Pishgar, M. R. K. Musa, S. M. S. Riyadh, M. Yu, G. Sumanasekera, and J. B. Jasinski, *npj 2D Mater Appl.* **5**, 30 (2021).
- [57] N. L. Nair, E. Maniv, C. John, S. Doyle, J. Orenstein, and J. G. Analytis, *Nat. Mater.* **19**, 153 (2020).
- [58] A. Little, C. Lee, C. John, S. Doyle, E. Maniv, N. L. Nair, W. Chen, D. Rees, J. W. Venderbos, R. M. Fernandes *et al.*, *Nat. Mater.* **19**, 1062 (2020).
- [59] See Supplemental Material at <http://link.aps.org/supplemental/10.1103/PhysRevMaterials.5.054002> for details of DFT calculations and AIMD simulations; pristine (GeP₃)_{BL} and Cr-doping configurations; formation energy and planar average spin-density equations; lower doping concentration.
- [60] V. Korobtsov, V. Lifshits, and A. Zotov, *Surf. Sci.* **195**, 466 (1988).
- [61] A. B. McLean, L. J. Terminello, and F. J. Himpsel, *Phys. Rev. B* **41**, 7694 (1990).
- [62] D. P. Andrade, R. H. Miwa, B. Drevniok, P. Drage, and A. B. McLean, *J. Phys. Condens. Matter* **27**, 125001 (2015).
- [63] J. Choe, K. Lee, C.-L. Huang, N. Trivedi, and E. Morosan, *Phys. Rev. B* **99**, 064420 (2019).
- [64] S. Mangelsen, J. Hansen, P. Adler, W. Schnelle, W. Bensch, S. Mankovsky, S. Polesya, and H. Ebert, *J. Phys. Chem. C* **124**, 24984 (2020).
- [65] G. Tenasini, E. Martino, N. Ubrig, N. J. Ghimire, H. Berger, O. Zaharko, F. Wu, J. F. Mitchell, I. Martin, L. Forró, and A. F. Morpurgo, *Phys. Rev. Research* **2**, 023051 (2020).
- [66] X.-C. Liu, S. Zhao, X. Sun, L. Deng, X. Zou, Y. Hu, Y.-X. Wang, C.-W. Chu, J. Li, J. Wu *et al.*, *Sci. Adv.* **6**, eaay4092 (2020).
- [67] X.-L. Qiu, J.-F. Zhang, Z.-Y. Lu, and K. Liu, *J. Phys. Chem. C* **123**, 24698 (2019).
- [68] L. Zhang, Y. Tang, A. R. Khan, M. M. Hasan, P. Wang, H. Yan, T. Yildirim, J. F. Torres, G. P. Neupane, Y. Zhang, Q. Li, and Y. Lu, *Adv. Sci.* **7**, 2002697 (2020).
- [69] J. Kudrnovský, I. Turek, V. Drchal, F. Máca, P. Weinberger, and P. Bruno, *Phys. Rev. B* **69**, 115208 (2004).
- [70] H. Shi, H. Pan, Y.-W. Zhang, and B. I. Yakobson, *Phys. Rev. B* **88**, 205305 (2013).
- [71] P. D. Reyntjens, S. Tiwari, M. L. Van de Put, B. Sorée, and W. G. Vandenberghe, *2D Materials* **8**, 025009 (2020).
- [72] P. Giannozzi, S. Baroni, N. Bonini, M. Calandra, R. Car, C. Cavazzoni, D. Ceresoli, G. L. Chiarotti, M. Cococcioni, I. Dabo, A. Dal Corso, S. de Gironcoli, S. Fabris, G. Fratesi, R. Gebauer, U. Gerstmann, C. Gougoussis, A. Kokalj, M. Lazzeri, L. Martin-Samos, N. Marzari, F. Mauri, R. Mazzarello, S. Paolini, A. Pasquarello, L. Paulatto, C. Sbraccia, S. Scandolo, G. Sclauzero, A. P. Seitsonen, A. Smogunov, P. Umari, and R. M. Wentzcovitch, *J. Phys.: Condens. Matter* **21**, 395502 (2009).
- [73] J. P. Perdew, K. Burke, and M. Ernzerhof, *Phys. Rev. Lett.* **77**, 3865 (1996).
- [74] T. Thonhauser, S. Zuluaga, C. A. Arter, K. Berland, E. Schröder, and P. Hyldgaard, *Phys. Rev. Lett.* **115**, 136402 (2015).
- [75] T. Thonhauser, V. R. Cooper, S. Li, A. Puzder, P. Hyldgaard, and D. C. Langreth, *Phys. Rev. B* **76**, 125112 (2007).
- [76] K. Berland, V. R. Cooper, K. Lee, E. Schröder, T. Thonhauser, P. Hyldgaard, and B. I. Lundqvist, *Rep. Prog. Phys.* **78**, 066501 (2015).
- [77] D. Langreth, B. I. Lundqvist, S. D. Chakarova-Käck, V. Cooper, M. Dion, P. Hyldgaard, A. Kelkkanen, J. Kleis, L. Kong, S. Li *et al.*, *J. Phys.: Condens. Matter* **21**, 084203 (2009).
- [78] S. L. Dudarev, G. A. Botton, S. Y. Savrasov, C. J. Humphreys, and A. P. Sutton, *Phys. Rev. B* **57**, 1505 (1998).
- [79] P. E. Blöchl, *Phys. Rev. B* **50**, 17953 (1994).
- [80] G. Kresse and J. Furthmüller, *Phys. Rev. B* **54**, 11169 (1996).